2020

Bacteriophage SP01 gene product 56 inhibits Bacillus subtilis cell division by interacting with FtsL and disrupting Pbp2B and FtsW recruitment

Amit Bhambhani

Isabella Iadicicco

Jules Lee

Syed Ahmed

Max Belfatto

See next page for additional authors

Authors

Amit Bhambhani, Isabella Iadicicco, Jules Lee, Syed Ahmed, Max Belfatto, David Held, Alexia Marconi, Aaron Parks, Charles R Stewart, William Margolin, Petra Anne Levin, and Daniel P Haeusser

AMERICAN SOCIETY FOR MICROBIOLOGY | Journal of Bacteriology®

RESEARCH ARTICLE

Bacteriophage SP01 Gene Product 56 Inhibits *Bacillus subtilis* Cell Division by Interacting with FtsL and Disrupting Pbp2B and FtsW Recruitment

Amit Bhambhani,[a] Isabella Iadicicco,[a] Jules Lee,[a] Syed Ahmed,[a] Max Belfatto,[a] David Held,[a] Alexia Marconi,[a] Aaron Parks,[a] Charles R. Stewart,[b] William Margolin,[c] Petra Anne Levin,[d] Daniel P. Haeusser[a]

[a]Biology Department, Canisius College, Buffalo, New York, USA
[b]Department of BioSciences, Rice University, Houston, Texas, USA
[c]Department of Microbiology and Molecular Genetics, McGovern Medical School, University of Texas, Houston, Texas, USA
[d]Department of Biology, Washington University in St. Louis, St. Louis, Missouri, USA

Amit Bhambhani, Isabella Iadicicco, and Jules Lee contributed equally to the work. Author order was determined alphabetically by last name and seniority (time spent in the laboratory).

ABSTRACT Previous work identified gene product 56 (gp56), encoded by the lytic bacteriophage SP01, as being responsible for inhibition of *Bacillus subtilis* cell division during its infection. Assembly of the essential tubulin-like protein FtsZ into a ring-shaped structure at the nascent site of cytokinesis determines the timing and position of division in most bacteria. This FtsZ ring serves as a scaffold for recruitment of other proteins into a mature division-competent structure permitting membrane constriction and septal cell wall synthesis. Here, we show that expression of the predicted 9.3-kDa gp56 of SP01 inhibits later stages of *B. subtilis* cell division without altering FtsZ ring assembly. Green fluorescent protein-tagged gp56 localizes to the membrane at the site of division. While its localization does not interfere with recruitment of early division proteins, gp56 interferes with the recruitment of late division proteins, including Pbp2b and FtsW. Imaging of cells with specific division components deleted or depleted and two-hybrid analyses suggest that gp56 localization and activity depend on its interaction with FtsL. Together, these data support a model in which gp56 interacts with a central part of the division machinery to disrupt late recruitment of the division proteins involved in septal cell wall synthesis.

IMPORTANCE Studies over the past decades have identified bacteriophage-encoded factors that interfere with host cell shape or cytokinesis during viral infection. The phage factors causing cell filamentation that have been investigated to date all act by targeting FtsZ, the conserved prokaryotic tubulin homolog that composes the cytokinetic ring in most bacteria and some groups of archaea. However, the mechanisms of several phage factors that inhibit cytokinesis, including gp56 of bacteriophage SP01 of *Bacillus subtilis*, remain unexplored. Here, we show that, unlike other published examples of phage inhibition of cytokinesis, gp56 blocks *B. subtilis* cell division without targeting FtsZ. Rather, it utilizes the assembled FtsZ cytokinetic ring to localize to the division machinery and to block recruitment of proteins needed for septal cell wall synthesis.

KEYWORDS *Bacillus subtilis*, cell division, FtsZ, SP01

Most bacteria initiate cytokinesis through regulated assembly of the conserved tubulin-like GTPase FtsZ at the future site of division. FtsZ assembles into a toroidal array of treadmilling polymers that serve as a platform for recruitment of the

Citation Bhambhani A, Iadicicco I, Lee J, Ahmed S, Belfatto M, Held D, Marconi A, Parks A, Stewart CR, Margolin W, Levin PA, Haeusser DP. 2021. Bacteriophage SP01 gene product 56 inhibits *Bacillus subtilis* cell division by interacting with FtsL and disrupting Pbp2B and FtsW recruitment. J Bacteriol 203:e00463-20. https://doi.org/10.1128/JB.00463-20.

Editor Yves V. Brun, Université de Montréal

Address correspondence to Daniel P. Haeusser, haeussed@canisius.edu.

Received 12 August 2020
Accepted 29 September 2020
Accepted manuscript posted online 19 October 2020
Published 18 December 2020

cell division machinery, including enzymes needed for septal cell wall synthesis (1). Proper placement of the FtsZ ring in time and space is required to ensure that newborn cells reach adequate size and contain a full genetic complement. To achieve this, FtsZ assembly at midcell and subsequent division are highly precise, with a <1% margin of error, suggesting a highly regulated process (2, 3). Blocking FtsZ assembly prevents membrane invagination and septal cell wall synthesis, leading to filamentous, multinucleated cells and eventual cell death (4).

As a conserved protein that is essential for division in most bacteria, FtsZ is an appealing target of study both for understanding its regulation and for potential development of novel antibiotics (5–7). Regulators of FtsZ assembly encoded within the *Escherichia coli* genome include factors originally derived from phages. These include *dicB* and *dicF* of the cryptic phage Qin (aka phage Kim) and the *kilR* (*orfE*) gene of the cryptic phage Rac (8). The RNA product of *dicF* binds to *ftsZ* mRNA to inhibit its translation (9), while the DicB peptide interacts with the FtsZ inhibitor MinC (10) to target ring assembly independent of its normal regulator MinD but dependent on ZipA (11). Transient division inhibition by cryptic DicB benefits the host by inhibiting phage receptor proteins ManY and ManZ, enhancing immunity to bacteriophage λ infection by up to 100-fold (12). The KilR peptide of Rac inhibits *E. coli* division through an unknown Min-independent mechanism that also causes increased loss of rod shape, although the benefit of this is less clear (13).

Functional bacteriophages also appear to encode factors that transiently block host cell division during infection. Expression of the 0.4 gene of T7 phage or *kil* of λ phage leads to *E. coli* cell filamentation through direct interference with FtsZ assembly by their protein products (14–16). In both cases, temporary inhibition of host cytokinesis by the phage prior to host lysis results in a subtle competitive advantage for the virus, although the specific nature of these advantages remains unclear.

Although all of the aforementioned factors come from phages that infect *E. coli*, it is likely that cytokinesis serves as a target for phages in the majority of other bacterial species as well. One reported example exists for the model Gram-positive species *Bacillus subtilis* and its lytic bacteriophage SP01. SP01 *orf56* lies in an operon comprising genes 58 through 56 (17). Expression of *orf56* alone, or in the context of the entire operon, leads to *B. subtilis* filamentation and death (18), but the mechanism behind this inhibition of cytokinesis is unknown.

The players involved in *B. subtilis* cytokinesis share commonalities with those involved in the *E. coli* division machinery, but several distinctions also exist (19, 20). Assembly of FtsZ at the membrane in *B. subtilis* involves interaction with the well-conserved FtsA and with SepF, each of which contains a membrane-targeting sequence (21). The nonessential transmembrane protein EzrA, an inhibitor of FtsZ assembly at the cell poles (22), also plays a separate role as part of the early division machinery to help maintain FtsZ assembly dynamics (23). Subsequent steps include recruitment of a trio of closely interacting, membrane-spanning proteins, DivIB, FtsL, and DivIC. While *divIB* is dispensable in *B. subtilis* under laboratory conditions, both *ftsL* and *divIC* are essential for cytokinesis (24–26). Cellular levels of DivIB, FtsL, and DivIC are interdependent, closely linked through targeted proteolysis (27, 28). DivIB, FtsL, and DivIC cooperatively function as a complex to recruit the transpeptidase Pbp2B and the transglycosylase FtsW, both essential for septal cell wall synthesis (29).

Here, we characterize the activity of SP01 gene product 56 (gp56) in inhibition of *B. subtilis* cell division. We find that, unlike all previously identified phage-derived inhibitors of cytokinesis, gp56 inhibits division without blocking FtsZ assembly. Instead, gp56 localizes to the *B. subtilis* division machinery in an FtsZ-dependent manner, where it inhibits recruitment of later division components needed for septal cell wall synthesis. Our results suggest that localization of gp56 to the site of division involves disruptive interactions with FtsL that lead to reduced recruitment of Pbp2B and FtsW, resulting in cell filamentation and death.

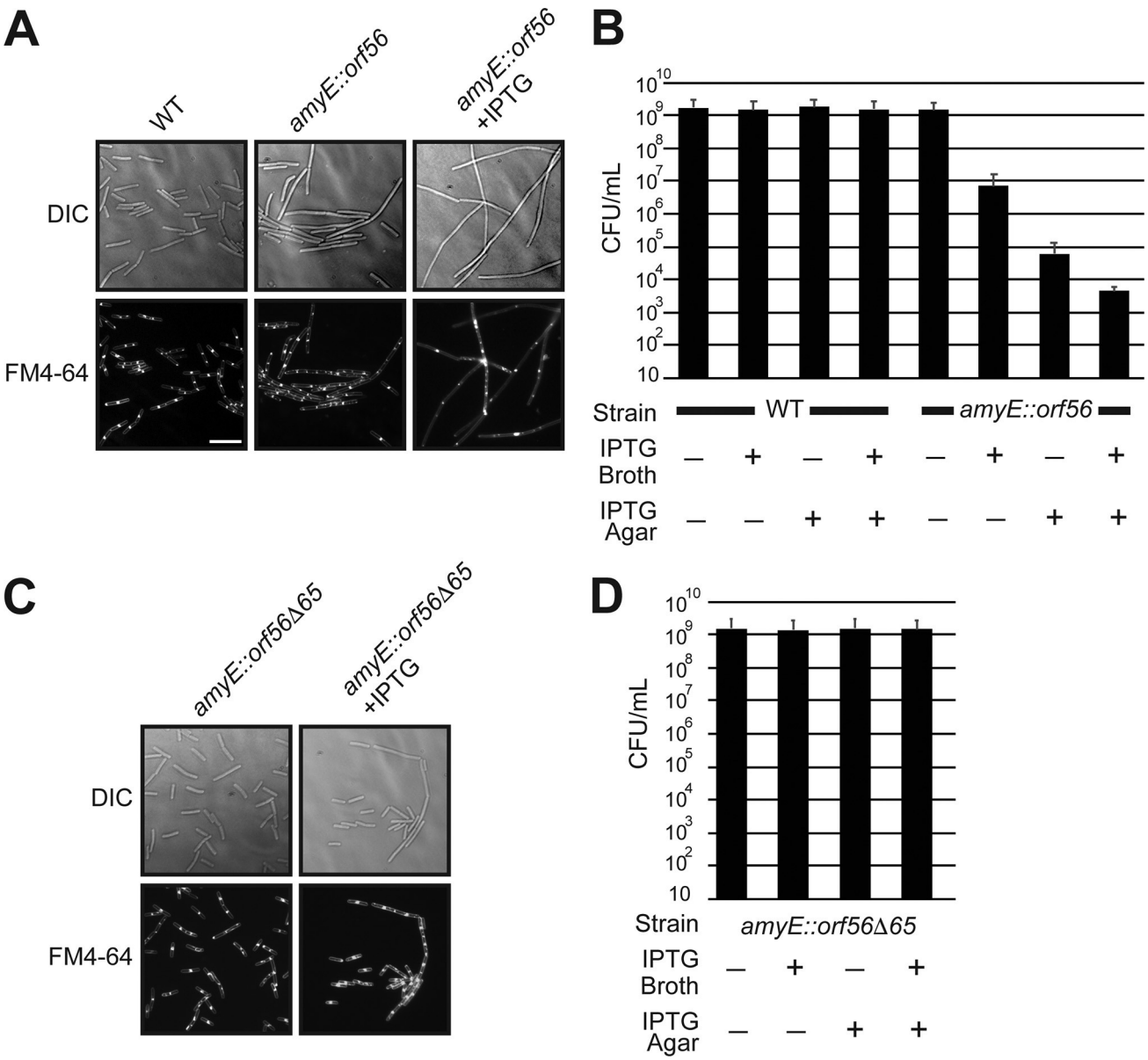

FIG 1 gp56 inhibits *B. subtilis* cell division. (A and C) Representative micrographs of live JH642 (WT), DPH102 (*amyE*::*orf56*), and DPH175 (*amyE*::*orf56*Δ*65*) cells from mid-log-phase cultures (see Materials and Methods) grown in LB medium with or without 1 mM IPTG, as indicated, for induction of chromosomally placed *orf56* or *orf56*Δ*65* at the *amyE* locus. DIC shows cells in bright-field (top row), and FM4-64 fluorescence staining (bottom row) shows cell membranes to differentiate between undivided individual cell filaments and multiple chained cells that form in the JH642 background with septal FM4-64 staining. Scale bar = 5 μm. (B and D) CFU per milliliter from plating efficiency assays using dilutions of strains as in panels A and C, taken from mid-log-phase cultures grown in LB medium with or without 1 mM IPTG, as indicated, and plated on either LB agar (left) or LB agar with 1mM IPTG (right). Values are averages from three separate trials, with standard deviations shown in error bars.

RESULTS

Single-copy, chromosomal expression of SP01 bacteriophage *orf56* inhibits *B. subtilis* cell division. The previous report of division inhibition by gp56 utilized a multicopy plasmid, pPW19. To determine whether gp56 is sufficient to inhibit division in single copy, we generated a strain, DPH102, in which *orf56* was expressed from a chromosomally encoded, isopropyl-β-D-thiogalactopyranoside (IPTG)-induced promoter at the amylase locus of *B. subtilis* strain JH642. Induction of *orf56* in DPH102 resulted in cell filamentation (Fig. 1A) similar to that previously reported in the *B. subtilis* CB10 background using pPW19 (18). Consistent with division inhibition, staining the cell membrane with FM4-64 indicated that filaments were generally aseptate, with the

exception of occasional septa at midcell. Such septa often appeared broader and ill formed, consistent with a division block.

For verification purposes, we additionally repeated published results from plasmid-borne *orf56* expression (18) but in our JH642 background. We transformed JH642 with pAP1 (pPW19 with the entire gene 58 through 56 operon) or pAP6 (pPW19 with *orf56* alone) to generate DPH176 and DPH3, respectively. As previously reported for the CB10 background, IPTG induction of the operon or *orf56* alone inhibited JH642 *B. subtilis* cell division indistinguishably, without altering cell growth or DNA replication/segregation (see Fig. S1 in the supplemental material).

CFU counts from plating efficiency assays of serial dilutions verified the lethality of long-term division inhibition, while also showing the reversibility of short-term division inhibition upon return to growth conditions without continued *orf56* induction. Mid-log-phase cultures of DPH102 diluted in LB IPTG agar showed 4- to 5-log-unit reductions in CFU after being pregrown in LB or LB IPTG liquid medium. However, cells expressing gp56 in liquid culture could be partially restored to growth once plated on LB agar without IPTG (Fig. 1B).

B. subtilis typically grows for ~4 to 5 mass doublings in the absence of division (e.g., in the presence of gp56) before growth plateaus and cells enter a viable but nonculturable state (30). Consistent with the previous gp56 report (18), division inhibition by gp56 did not significantly alter these short-term *B. subtilis* growth rates. Under our growth conditions, JH642 had a generation time (T_D) of 29.0 ± 1.1 min. Uninduced DPH102 had a similar T_D of 28.3 ± 0.5 min, while induced DPH102 expressing gp56 had a T_D of 30.7 ± 2.2 min. Similarly, DNA staining verified that DNA replication and segregation appeared unaffected in DPH102 with or without IPTG (data not shown), consistent with previous reports of gp56 expression and Fig. S1.

The carboxyl-terminal domain of gp56 is essential for division inhibition. To identify regions of gp56 required for division inhibition, we serially passaged DPH3 (JH642 with pAP6) on LB IPTG agar to isolate suppressors that grow in the presence of gp56. Plasmid sequencing revealed that the overwhelming majority of such isolates had either promoter mutations or nonsense mutations early in the gene 56 coding sequence. One isolate (*orf56Δ65*), however, contained a nonsense mutation at codon 65 of the gene, truncating the predicted gp56Δ65 product by 15 of 79 residues. Analysis of the primary sequence of gp56 by SMART (31) predicts that residues 37 to 59 form a transmembrane domain, with a highly favored orientation prediction by TMpred (32) in which its amino terminus faces the cytoplasm and its carboxyl terminus faces extracellularly.

To assess the phenotype of gp56Δ65 in comparison with the wild-type (WT) cells, we subcloned the *orf56Δ65* allele from its isolated plasmid (pDH89) and placed it under IPTG-inducible control at the *amyE* locus of JH642 to generate DPH175. As expected, single-copy, chromosomal expression of gp56Δ65 failed to cause cell filamentation (Fig. 1C) or a decrease in CFU (Fig. 1D). This suggests that gp56Δ65 has lost its ability to inhibit *B. subtilis* cell division, and it implicates the predicted extracellular C terminus of gp56 as essential for mediating that inhibitory phenotype.

Division inhibition by gp56 is independent of FtsZ ring formation. Previously characterized bacteriophage division inhibitors function by reducing cellular FtsZ concentrations (e.g., *dicF*) (9) or by directly antagonizing its assembly (e.g., *kil*) (15, 16). To determine whether the same is the case for gp56, we used immunofluorescence microscopy (IFM) to localize FtsZ in WT, DPH102, and DPH175 cells in the presence and absence of inducer.

As expected for the JH642 WT background, the majority of cells displayed a single FtsZ ring at midcell (Fig. 2A), with an average cell length of 4.1 μm and width of 1.3 μm (Fig. 2B and C). Similar to WT cells, uninduced DPH102 cells contained single, medial FtsZ rings (Fig. 2A) with an average cell length of 4.5 μm and width of 1.4 μm (Fig. 2B and C). As expected, expression of gp56 in DPH102 resulted in a division block, increasing the average cell length to ~18.6 μm (Fig. 2B). The average length measure-

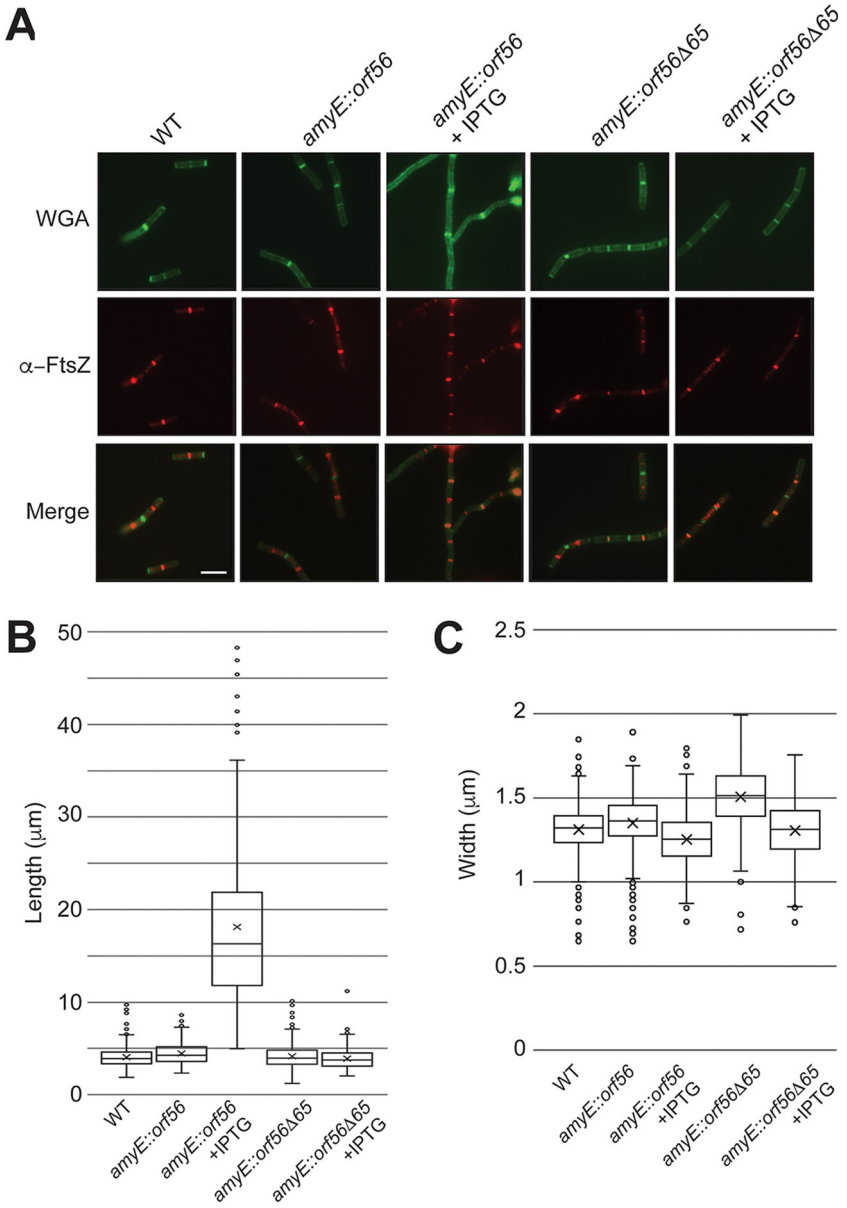

FIG 2 gp56 does not inhibit FtsZ ring assembly in *B. subtilis*. (A) Representative false-colored immunofluorescence micrographs of glutaraldehyde/paraformaldehyde-fixed JH642 (WT), DPH102 (*amyE*::*orf56*), and DPH175 (*amyE*::*orf56Δ65*) cells taken from mid-log-phase cultures with or without 1 mM IPTG as indicated. Fluorescent wheat germ agglutinin (WGA) staining (top row) shows the cell wall, and anti-FtsZ (middle row) shows the signal from fluorescence marker-conjugated secondary antibody to the primary antibody against FtsZ. Merge (bottom row) shows a merge of the WGA and anti-FtsZ signals. (B) Scatter-box plots of cell length quantification ($n > 100$) of strains from panel A. Box borders denote upper and lower quartiles, with the horizontal line in the box depicting the median and X depicting the mean. Whiskers show upper and lower deviations of data. (C) Scatter-box plots of cell width quantification ($n > 100$) of strains from panel A, with data shown as in panel B.

ment of these filaments is likely an underestimate, as many filaments extended past the micrograph field of view. Somewhat surprisingly, we observed regularly spaced FtsZ rings along the length of DPH102 cells cultured in the presence of IPTG (Fig. 2A). As expected, almost all DPH175 cells contained a single FtsZ ring at midcell (Fig. 2A) regardless of gp56Δ65 expression. Additionally, DPH175 fixed cell lengths were not altered by expression of the truncated gp56Δ65 (4.2 versus 3.9 μm) (Fig. 2B). Uninduced DPH175 cells did have a slightly larger average cell width (1.5 μm), compared to induced conditions (1.3 μm) or the other strains. While a statistically significant increase

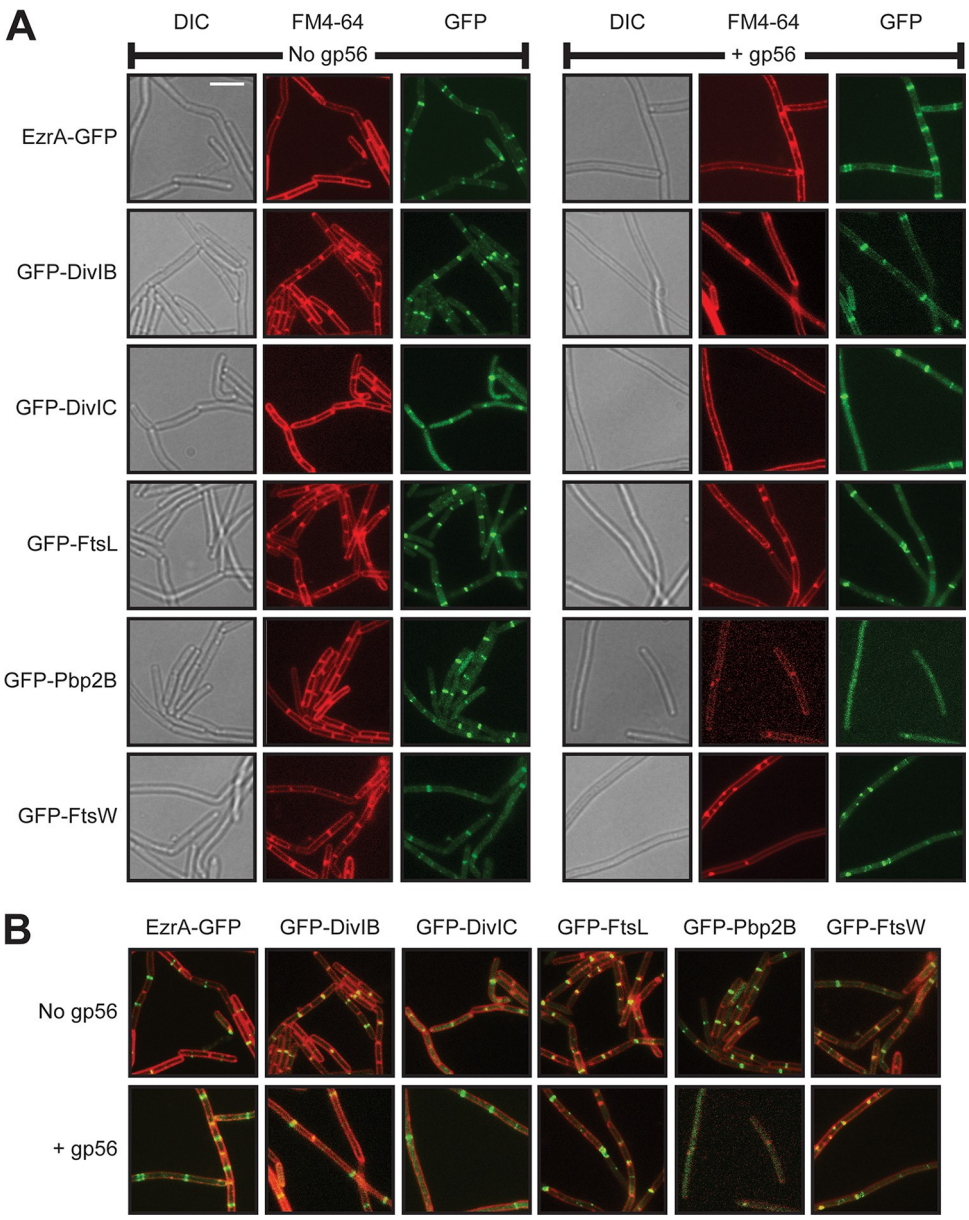

FIG 3 gp56 prevents recruitment of late, essential division proteins needed for *B. subtilis* septal cell wall synthesis. (A) Representative false-colored fluorescence micrographs of live cells of strains expressing EzrA-GFP (PL847 and DPH111), GFP-DivIB (DPH79 and DPH97), GFP-DivIC (DPH617 and DPH618), GFP-FtsL (DPH1108 and DPH584), GFP-Pbp2B (DPH414 and DPH415), or GFP-FtsW (DPH408 and DPH409) in the absence (left) or presence (right) of gp56. Each field of view includes a DIC image showing cells in bright-field, FM4-64 showing fluorescently stained membranes, and the GFP fluorescence signal showing localization of the indicated fusion construct. Scale bar = 5 μm. (B) Merged panels, on the same scale, of WGA and GFP signals from panel A.

by analysis of variance, we interpret this as a "bloating" artifact from the lysozyme treatment during IFM slide preparation using fixed cells (33). As seen in later figures of live cells, (e.g., EzrA-green fluorescent protein [GFP] in Fig. 3), no significant changes in width are otherwise apparent.

Although DPH102 filaments formed by gp56 expression still contain FtsZ rings, it is possible that they assemble less efficiently. Calculations of length/FtsZ ring (L/R) ratios in DPH102 filaments, compared to cells of normal length, allow determination of any alteration in FtsZ ring frequency or stability in the presence of gp56. Nonfilamentous cells had an average L/R ratio of 4.2. In contrast, filamentous DPH102 cells had an average L/R ratio of 7.2. This suggests that, while gp56 does not abolish FtsZ ring

assembly, it does somewhat reduce the rings. Regardless, such a modest increase in the L/R ratio would not explain the observed extreme filamentation.

***gp56* interferes with recruitment of essential late division proteins to the site of division.** Together, the preceding data indicate that gp56 acts to block cell division at a step following FtsZ ring formation. Preventing recruitment to FtsZ of other essential proteins of the division machinery, such as enzymes involved in septal peptidoglycan synthesis, also produces a filamentous cell phenotype. To identify the target of gp56, we assayed recruitment of individual GFP-tagged division components in the JH642 *amyE*::P_{spac}-*orf56* (DPH102) background, in the absence and presence of the inducer IPTG.

Our resulting data indicate that gp56-mediated division inhibition occurs through disruption of late protein localization. GFP fusions to the relatively early localized EzrA (DPH111) and to the later DivIB (DPH97) exhibited regular staining patterns in filaments formed from gp56 expression, comparable to those of cells lacking gp56 (Fig. 3).

We next constructed *gfp*-tagged fusions to *ftsW* and *pbp2b* and cloned these at the amylase locus under xylose control (DPH387 and DPH400, respectively). These strains were then transformed with pPW19 or pAP6 to assess potential gp56 effects on GFP-FtsW (DPH408 and DPH409) or GFP-Pbp2B (DPH414 and DPH415) localization. As later recruited proteins, fewer cells in the population normally contain localized GFP-FtsW or GFP-Pbp2B at any given time, compared to early recruited proteins that remain localized for most of the cell cycle. Nonetheless, in the absence of gp56, visible GFP-FtsW and GFP-Pbp2B bands were apparent at midcell in multiple cells within a given field of view. In contrast, in the presence of gp56, no cytoplasmic bands of GFP-Pbp2B were observed, and the only GFP-FtsW bands visible were less uniform in shape (Fig. 3; also see Fig. S2) and frequently overlapped blebs of improperly formed septal membrane visible through fluorescent FM4-64 staining (Fig. 3B).

The diminished recruitment of GFP-FtsW and GFP-Pbp2B by gp56 suggested that the phage peptide might interfere with formation of the DivIB-FtsL-DivIC complex, which cooperatively recruits FtsW and Pbp2B for cell wall septum formation (29). To test this possibility, we constructed *gfp*-tagged fusions to *ftsL* and *divIC* and inserted them at the amylase locus under xylose control (DPH579 and DPH614, respectively). These strains were then transformed with pPW19 or pAP6 to assess potential gp56 effects on GFP-FtsL (DPH1108 and DPH584) or GFP-DivIC (DPH617 and DPH618) localization.

Upon their induction, both GFP-FtsL and GFP-DivIC demonstrated localization to midcell in the absence of gp56, as expected. Additionally, GFP-FtsL and GFP-DivIC still were capable of localizing as cytoplasmic bands within cell filaments formed from gp56 expression. However, the localizations of FtsL or DivIC appeared reduced in the presence of gp56, compared to the absence of gp56. In particular, FtsL showed an occasional pattern of disrupted localization in helices, doublets, or blebs (Fig. 3; also see Fig. S2).

gp56 colocalizes with the division machinery in a manner that requires FtsZ, FtsA, and FtsL. An inhibitor of bacterial cell division that acts after FtsZ ring assembly might localize to midcell via interactions with components of the division machinery to prevent recruitment of relatively later components. To determine whether this is true for gp56 and the observed loss of FtsW and Pbp2B recruitment in its presence, we constructed a chromosomal fusion of *gfp* to *orf56* at the *amyE* locus under the control of xylose (DPH50). We chose an N-terminal GFP tag based on the prediction that the C-terminal end of the gp56 peptide would be extracellular and the N-terminal end intracellular. As a control, we also constructed a strain with a similar *gfp* fusion to the inactive *orf56Δ65* allele (DPH170).

Induction of *gfp-orf56* resulted in cells with a clear band of GFP fluorescence at midcell, consistent with GFP-gp56 localization to the divisome. In contrast, induction of the inactive truncated gp56 control showed poor to little localization (Fig. 4A). Notably, the addition of the GFP tag to the gp56 peptide does seem to interfere with the

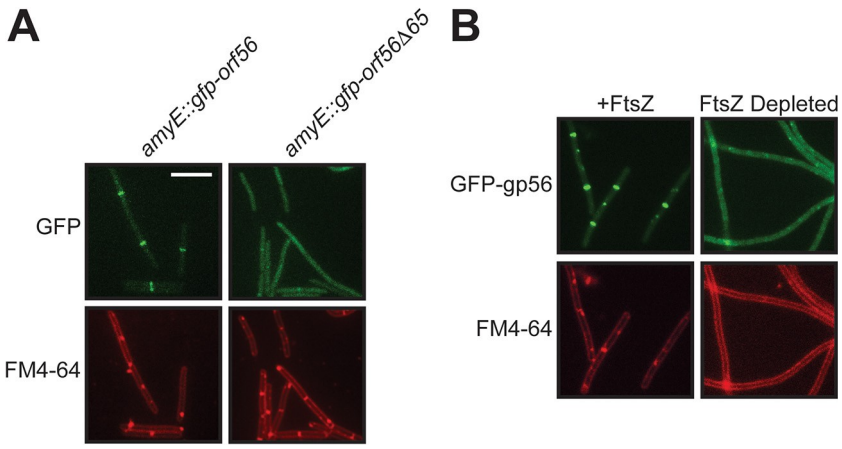

FIG 4 GFP-gp56 localizes to the *B. subtilis* site of division in an FtsZ-dependent manner. (A) Representative false-colored fluorescence micrographs of live DPH50 (*amyE*::*gfp-orf56*) and DPH170 (*amyE*::*gfp-orf56Δ65*) cells taken from mid-log-phase cultures with 0.1% xylose present to induce fusion protein expression. The GFP signal (top) shows fusion protein localization, and the FM4-64 fluorescence signal (bottom) shows cell membranes. Scale bar = 5 μm. (B) Representative false-colored fluorescence micrographs of live DPH504 (*ftsZ*::*spc xylA*::*tet thrC*::P_{xyl}-*ftsZ amyE*::P_{spac}-*gfp-orf56*) cells taken from mid-log-phase cultures with 1 mM IPTG present to induce GFP-gp56 in the presence (left) or absence (right) of xylose to express or to deplete FtsZ. The GFP signal (top) shows GFP-gp56 localization, and the FM4-64 fluorescence signal (bottom) shows cell membranes. Scale as in panel A.

peptide's activity in blocking cell division, as cells expressing *gfp-orf56* did not significantly filament.

To determine whether gp56 localization was dependent on FtsZ or downstream components of the divisome, we transformed the *amyE*::P_{xyl}-*gfp-orf56* region of the chromosome into strains that contain deletions, or permit depletion, of specific components of the cell division machinery. Depletion of *ftsZ* (DPH504) abolished GFP-gp56 localization to midcell (Fig. 4B), confirming that observed GFP-gp56 bands reflect localization to the site of division in a manner requiring the foundational assembled FtsZ.

We next sought to address what other components (if any in addition to FtsZ) were involved in recruitment of gp56 to its site of activity at the divisome. We first decreased/removed FtsA from the divisome by using a strain (DPH503) that permits depletion of the *ftsAZ* operon but continued expression of *ftsZ* alone at an ectopic locus while simultaneously inducing *gfp-orf56* expression. Not surprisingly, the resulting depletion of *ftsA* under these conditions also led to the loss of almost all GFP-gp56 localization. However, deletion of either *divIB* or *ezrA* (DPH55 and DPH177, respectively) did not result in any alteration of GFP-gp56 localization, compared to that seen in the WT background (Fig. 5).

Given these results and the observed loss of Pbp2B and FtsW localization in the presence of gp56, DivIC and FtsL are left as potential key factors that may contribute to gp56 recruitment to the divisome. Depletion of *divIC* resulted in a loss of the majority of GFP-gp56 fluorescent bands (Fig. 5; also see Fig. S3). Instead, GFP-gp56 signal mostly appeared at the periphery of cells (membrane localization) and in unproductive septal patches that appeared due to the filamentation of cells depleted of *divIC* (Fig. 5B). This argues that DivIC does play a significant role in gp56 recruitment to the divisome, although perhaps indirectly due to its link to FtsL levels. Similarly, depletion of *ftsL* (DPH1119) led to a loss in GFP-gp56 localization (Fig. 5; also see Fig. S3). Notably, however, this strain does not allow the depletion of *ftsL* alone but only in conjunction with *pbpB* (encoding Pbp2B), within the context of the *yllB-ylxA-ftsL-pbpB* operon. Because gp56 appears to prevent Pbp2B localization to the divisome, we would predict that depletion of *pbpB* alone should not lead to any loss of GFP-gp56 recruitment to the divisome. Indeed, following depletion of *pbpB* alone (DPH1121), GFP-gp56 retained its normal localization (Fig. 5; also see Fig. S3). This argues that the observed loss of its

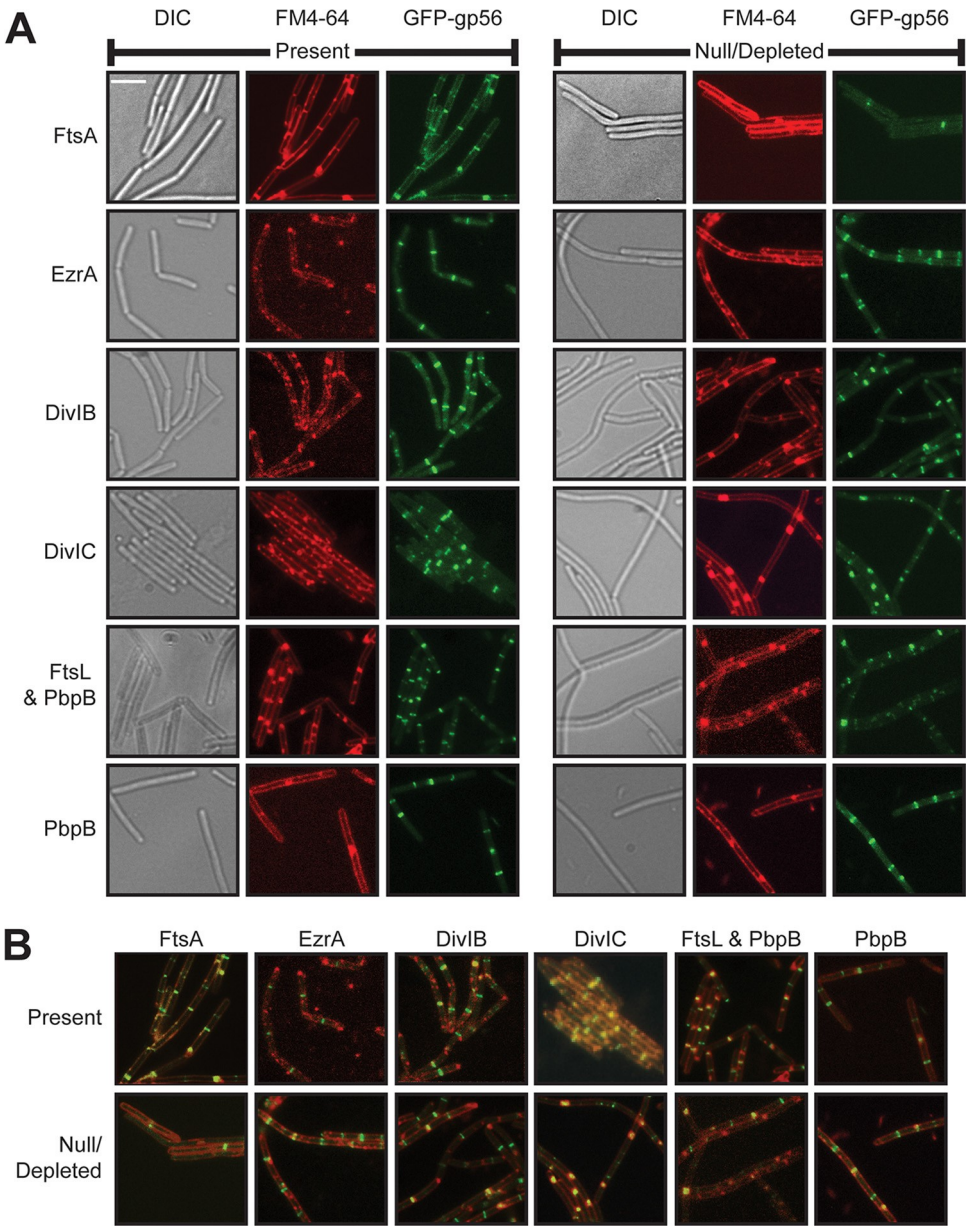

FIG 5 GFP-gp56 localization to the *B. subtilis* site of division requires DivIC/FtsL. (A) Representative false-colored fluorescence micrographs of live cells taken from mid-log-phase cultures containing (left) or missing (right) FtsA (DPH503), EzrA (JH642 or DPH55), DivIB (JH642 or DPH177), DivIC (DPH302), FtsL and Pbp2B in combination (DPH1121), or Pbp2B alone (DPH1119) through deletion/depletion. Each field of view includes a DIC image showing cells in bright-field, FM4-64 showing fluorescently stained membranes, and the GFP fluorescence signal showing localization of GFP-gp56. Scale bar = 5 μm. (B) Merged panels, on the same scale, of WGA and GFP signals from panel A.

localization following depletion of *ftsL* and *pbpB* together likely stems from the lack of FtsL specifically.

FtsL interacts with gp56 by bacterial two-hybrid assay. Observed disruptions in normal DivIC and FtsL localization in the presence of gp56, coupled with the observed dependence of gp56 localization on the presence of DivIC and FtsL, suggest that these three components might directly interact at the divisome. To test for potential interactions between these proteins, we cloned either *ftsL*, *divIC*, *orf56*, *orf56Δ65*, *divIB*, and *ftsW* into pKT25 and combined these in DHM1 cells also containing either *orf56*, *orf56Δ65*, or *ftsL* cloned into pUT18C. We then assayed the panels of paired genes for potential interaction of their expressed protein fusions with the bacterial two-hybrid

(BACTH) assay (34). Plating of the resulting strains on appropriate media containing X-Gal (5-bromo-4-chloro-3-indolyl-β-D-galactopyranoside) showed strong blue color production indicative of expected FtsL-FtsL and FtsL-DivIC interactions. Additionally, both combinations of gp56 with FtsL produced blue pigmentation, albeit relatively lighter (Fig. 6A). In contrast, gp56Δ65 indicated no interaction with FtsL in either combination.

We then assayed the relative strength of the interactions suggested above by growing the BACTH strains overnight in appropriate media to quantify β-galactosidase activities from lysates in an established assay using *o*-nitrophenol-β-galactoside (ONPG) reporter substrate. For this assay, activities >4 to 5-fold higher than baseline controls (~150 U/mg) are considered indicative of positive interaction (35). In agreement with qualitative results with plates containing X-Gal, FtsL demonstrated strong self-interaction and interaction with DivIC (5,197 U/mg and 3,175 U/mg, respectively). FtsL and gp56 additionally demonstrated β-galactosidase activity in both combinations (781 U/mg and 525 U/mg), >4-fold above negative controls with empty pKT25 (Fig. 6B). Similar to results with X-Gal, combinations of FtsL and gp56Δ65 showed β-galactosidase activities close to baseline.

DivIC overexpression suppresses gp56 inhibition of cell division. The aforementioned results are consistent with a model in which gp56 localizes to the divisome through interactions with FtsL (in turn dependent on FtsZ and FtsA). This interaction of FtsL with gp56 partially disrupts normal localization of FtsL and perhaps its interactions with DivIC. Thus, compromising the normal functions of FtsL and DivIC, this leads to decreased recruitment of Pbp2B and FtsW, thereby causing cell filamentation. We hypothesized that, if gp56 interacts with FtsL to disrupt its normal functions and interactions with DivIC, then perhaps overexpression of either of those components could dilute the inhibitory effects of gp56 and restore cell division.

While simultaneous overexpression of *ftsL* and *pbp2B* did not have any effect on gp56 inhibitory activity (data not shown), we found that overexpression of *divIC* through two separate constructs did suppress gp56 inhibition of cell division (Fig. 6C). In the first construct, we utilized a strain with an IPTG-inducible second copy of *divIC* at the amylase locus and transformed it with either pPW19 or pAP6. For the resulting strains (DPH660 and DPH661), IPTG addition simultaneously induced overexpression of *divIC* and gene 56 in pAP6. In contrast to the filamentation seen normally upon gp56 expression from pAP6, no cell filamentation occurred with the simultaneous overexpression of *divIC* (Fig. 6C), suggesting that extra DivIC is protective against gp56 activity. For the second construct, we utilized the *divIC* overexpression background with chromosomal expression of gene 56 from the *thrC* locus through xylose induction (DPH1152). When xylose alone was added to the resulting strain, gp56 expression led to cell filamentation as expected. However, inclusion of IPTG in addition to xylose allowed *divIC* overexpression and led to rescue from the gp56-mediated block in cell division (Fig. 6C). Together, these data support the model in which gp56 interferes with FtsL interactions with DivIC to block further divisome component recruitment, but additional cellular DivIC can dilute these gp56 effects.

DISCUSSION

The results reported here demonstrate that the inhibition of *B. subtilis* cell division by gp56 of bacteriophage SP01 is exerted downstream of FtsZ ring assembly. Together, our results suggest a model (Fig. 7) in which gp56 localizes to the division complex in an FtsAZ-dependent manner through interactions with FtsL, where its presence interferes with normal FtsL-DivIB interactions and activity, thereby reducing recruitment of Pbp2B and FtsW.

SP01 gp56 joins an expanding cast of phage-derived factors that inhibit host cytokinesis, including Kil of bacteriophage λ (15, 16), gp0.4 of bacteriophage T7 (14, 35), and elements of defective prophages like DicB (12), DicF of Qin (9), and Kil of Rac (13). Notably, however, SP01 gp56 is the first reported phage factor that does not target FtsZ either directly or indirectly to inhibit cytokinesis. Instead, gp56 has likely evolved to

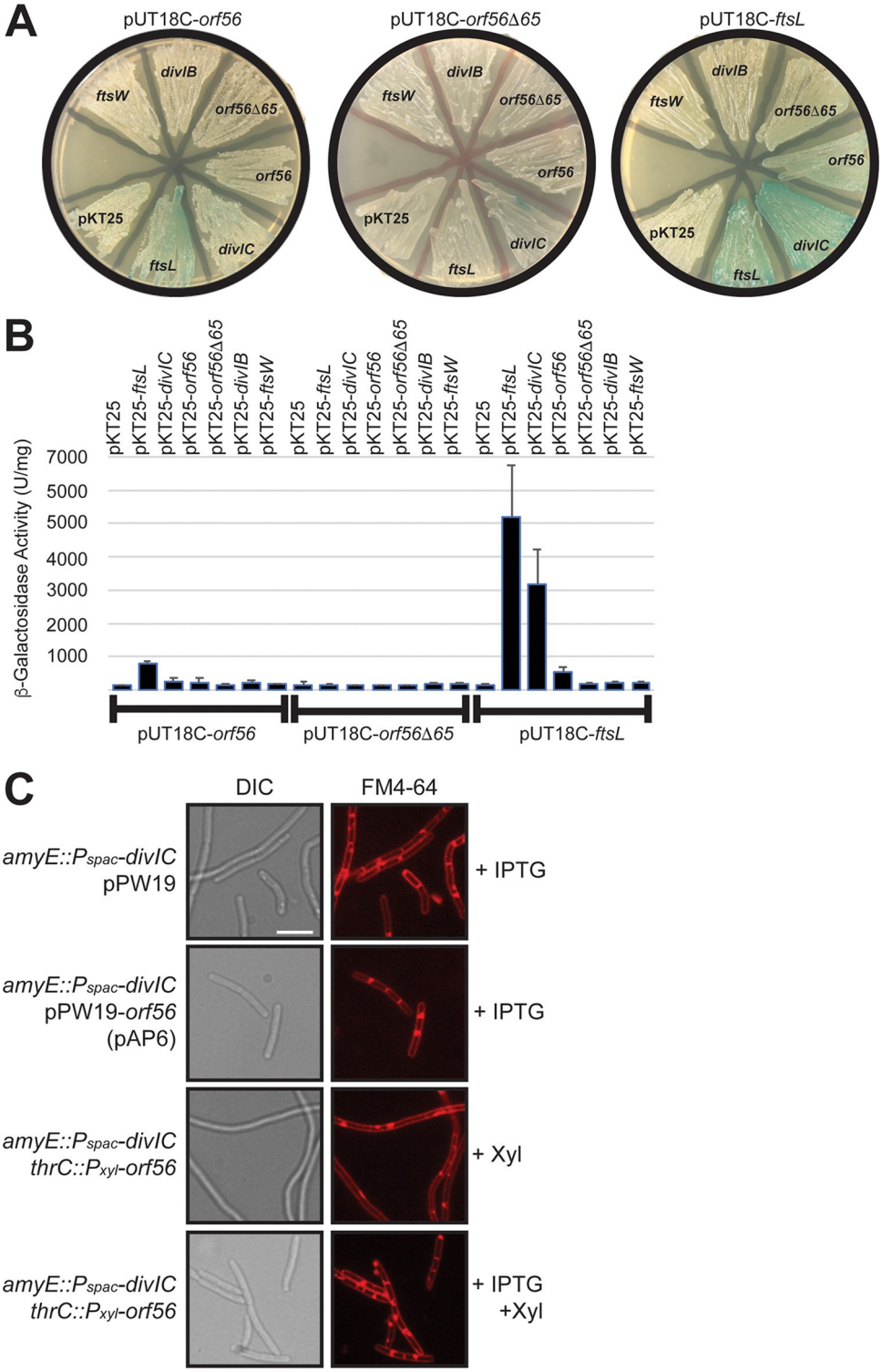

FIG 6 SP01 gp56 interacts FtsL and its activity is suppressed by *divIC* overexpression. (A) Photos of LB Amp^{100} Kan^{50} agar plates with 1 mM IPTG and 50 g/ml X-Gal, showing growth of DHM1 BACTH background *E. coli* strains harboring pUT18C-*orf56* (left), pUT18C-*orf56Δ65* (center), or pUT18C-*ftsL* (right) and a panel of indicated genes cloned in pKT25. (B) β-Galactosidase activities of the indicated BACTH plasmid combinations in strains as in panel A. Values are an average of three independent trials, with error bars representing standard deviations. (C) Representative false-colored fluorescence micrographs of live cells taken from mid-log-phase cultures, with DIC (left) showing cells in bright-field and FM4-64 (right) showing fluorescently stained membranes. DPH660 (*amyE*::P_{spac}-*divIC* pPW19) and DPH661 (*amyE*::P_{spac}-*divIC* pPW19-*orf56*) cells were grown with 1 mM IPTG to overexpress *divIC* and to express gene 56 from pPW19 (top two rows). DPH1152 (*amyE*::P_{spac}-*divIC thrC*::P_{xyl}-*orf56*) cells were grown with 0.1% xylose to express gene 56 in the absence (third row) or presence (bottom row) of 1 mM IPTG to overexpress *divIC*. Scale bar = 5 μm.

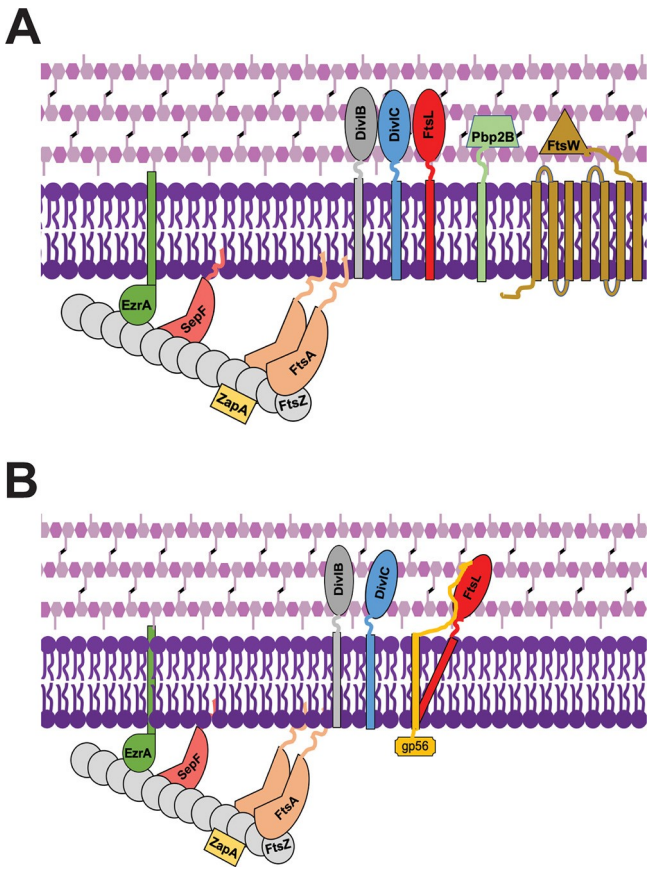

FIG 7 SP01 gp56 interacts with *B. subtilis* FtsL to disrupt the division machinery and to prevent recruitment of the Pbp2B and FtsW that are essential for septal cell wall synthesis. (A) Under normal conditions, the *B. subtilis* division machinery assembles into a cytokinesis-competent apparatus allowing for proper membrane constriction and septal wall synthesis. FtsZ polymers assemble at the membrane through interactions with membrane-associated FtsA, SepF, and EzrA. Stabilized by nonessential ZapA, assembled FtsZ and its membrane-associated partners allow recruitment of DivIB-FtsL-DivIC complexes that in turn help recruit Pbp2B and FtsW. (B) In the presence of SP01 gp56, the phage peptide interacts with FtsL, mildly disrupting its normal localization and its interaction with DivIC, preventing the normal recruitment of Pbp2B and FtsW. While lack of this late recruitment would also normally lead to rapid loss of the DivIB-DivIC-FtsL complex, its interaction with gp56 prevents their loss, effectively freezing the division machinery in a midassembled state that is unable to constrict or to build the septal cell wall, thereby leading to cell filamentation and death.

block subsequent recruitment of septal cell wall synthesis enzymes. A similar mechanism appears to have evolved in *B. subtilis* with the SOS-induced division inhibitor YneA, which likewise blocks cytokinesis downstream of FtsZ ring assembly (36).

In the case of SP01 gp56, this strategy also allows the bacteriophage to potentially exploit a nonfunctional division machinery platform for localization of its own factors. In a somewhat similar case, *B. subtilis* bacteriophage ϕ29 p1 protein localizes to assembled FtsZ rings at midcell to promote phage particle assembly (37) and depends on FtsZ, but not Pbp2B, for its localization. It is not yet known whether p1 interacts directly with FtsZ or utilizes another division protein for its localization like gp56. Regardless of its precise interactions, ϕ29 p1 recruitment to the division machinery only modestly interferes with *B. subtilis* cytokinesis (37), unlike the total block in division caused by SP01 gp56.

Within the SP01 genome, *orf56* is found at the end of an operon with genes 58 and 57 (17, 18), two genes whose products also lack any homologs in databases and whose function is unknown. It is possible that the products of these other genes colocalize along with gp56 to the FtsZ ring to carry out an activity for SP01 processing, similar to that seen with ϕ29 p1, that transiently delays cytokinesis sufficiently to prevent division

septum formation from interfering with assembling viral particles. It should be emphasized that *B. subtilis* encodes a transient division inhibitor during its SOS response (YneA) to permit DNA repair (36) or during the transition from vegetative growth to sporulation via RefZ activity on FtsZ (38, 39).

The previous study (18) identifying SP01 gp56 as an inhibitor of *B. subtilis* cytokinesis demonstrated that a temporary block in division does indeed occur during SP01 infection prior to host cell lysis. However, SP01 lacking *orf56* displays no apparent phenotypic defect in burst size or latency under laboratory conditions (18). Nonetheless, it is possible that gp56-mediated cytokinetic blocks provide subtle competitive advantages to SP01 under particular growth conditions by preventing cells from dividing over phage particles in the process of assembly. Lower levels of gp56 during SP01 infection may also slow division to take advantage of the vulnerability in cell integrity created at the site of division during cell wall remodeling. Experiments using phage competition assays and/or submaximal loads of infection may thus reveal competitive advantages for SP01with gp56.

Beyond the roles for gp56 in SP01 biology, its apparent interaction with FtsL makes it a potential tool for further study of the role of FtsL in *B. subtilis* cell division, as well as study of the effects of inhibiting Pbp2B and FtsW activity at midcell. Normally, loss of Pbp2B or FtsW localization to the division machinery perturbs "back-recruitment" of the ternary complex of DivIB-FtsL-DivIC, where they too become delocalized (27–29). In the presence of gp56, however, loss of Pbp2B and FtsW does not result in that perturbation, presumably because FtsL interactions with gp56 help protect it from proteolysis, even while rendering it at least partially dysfunctional.

The gp56-FtsL interaction observed here by BACTH assay is much weaker than FtsL-FtsL and FtsL-DivIC interactions, although still above the standard cutoff value for concluding evidence of interaction. One possibility is that the gp56 fusion used for this assay is partially nonfunctional, like GFP-gp56. It may also be that gp56 can outcompete DivIC for interaction with FtsL, despite the relatively weak gp56-FtsL interaction. Cellular levels of gp56 during SP01 infection and our conditions are unknown, but they may surpass those of DivIC. This would be consistent with the ability of overproduced DivIC to rescue the gp56-mediated division block by outcompeting gp56.

Recent studies from *E. coli* suggest that FtsQ, FtsL, and FtsB (homologs of DivIB, FtsL, and DivIC, respectively) together help bridge the activity of the earlier recruited FtsA with the later proteins needed for septum synthesis and invagination of the Gram-negative outer membrane (40, 41). Despite lacking an outer membrane, a similar type of communication between early and late division proteins might be mediated by DivIB, FtsL, and DivIC in *B. subtilis*. Consistent with this, we have isolated a spontaneous suppressor of gp56-mediated cell division inhibition that maps to *ftsA*. Although gp56 still localizes to the site of division in the presence of this FtsA suppressor, it appears that the mutant FtsA is capable of stabilizing DivIB, FtsL, and DivIC components sufficiently to permit Pbp2B and FtsW recruitment despite the presence of gp56 (unpublished data.) Alternatively, by analogy to the stronger recruitment of the key late *E. coli* divisome protein FtsN by hypermorphic alleles of FtsA (42–44), our FtsA mutant may be able to bypass the DivIB/FtsL/DivIC requirement for recruitment of Pbp2/FtsW. The characterization of this gp56-resistant *ftsA* mutant allele and further study of the role that genes 58 to 56 might play in SP01 biology will be the focus of our future studies.

MATERIALS AND METHODS

Bacterial strains and growth conditions. All *B. subtilis* and *E. coli* strains used are listed in Table 1. *B. subtilis* strains used for experiments are derivatives of JH642 (45). *E. coli* strain AG1111 (46) was used for plasmid construction and storage, and DHM1 (34) was used for BACTH analysis.

Cells were grown in, or on, LB Lennox medium (1% tryptone, 0.5% yeast extract, 0.5% NaCl, 0.35 K_2HPO_4 [pH 7.4]) (Teknova) at 30°C for temperature-sensitive strains (GFP fusions) under permissive conditions or at 37°C for other strains. Antibiotic concentrations were as described previously (23, 47). As appropriate, 1 mM IPTG (Gold Biotechnology) was used for induction of the P_{spac} promoter or its derivatives, and 0.5% D-(+)-xylose (Hitech) was used for induction of the P_{xyl} promoter.

TABLE 1 Bacterial strains used in this study

Strain name	Species	Genotype	Source or reference	Plasmid intermediate[a]
AIG184	*B. subtilis*	JH642 *yllB*::P_{spachy}-*yllB-ylxA-ftsL-pbpB cat*	A. Grossman	NA
AIG23	*B. subtilis*	JH642 *ftsL*::P_{spac}-*ftsL-pbpB cat*	A. Grossman	NA
BW121	*B. subtilis*	JH642 *ftsZ*::*spc xylA*::*tet thrC*::P_{xyl}-*ftsZ erm*	53	NA
DPH102	*B. subtilis*	JH642 *amyE*::P_{spac}-*orf56 cat*	This study	pDH83
DPH105	*B. subtilis*	JH642 *divIB*::*cat*	This study	NA
DPH1108	*B. subtilis*	DPH579/pPW19	This study	NA
DPH111	*B. subtilis*	PL847 *amyE*::P_{spac}-*orf56 cat*	This study	NA
DPH1119	*B. subtilis*	AIG23 *amyE*::P_{xyl}-*gfp-orf56 cat*::*spc*	This study	NA
DPH1121	*B. subtilis*	AIG184 *amyE*::P_{xyl}-*gfp-orf56 cat*::*spc*	This study	NA
DPH1152	*B. subtilis*	DPH648 *thrC*::P_{xyl}-*orf56 erm*	This study	NA
DPH162	*B. subtilis*	DPH50 *cat*::*spc*	This study	NA
DPH170	*B. subtilis*	JH642 *amyE*::P_{xyl}-*gfp-orf56Δ65 cat*	This study	pDH91
DPH175	*B. subtilis*	JH642 *amyE*::P_{spac}-*orf56Δ65 cat*	This study	pDH92
DPH176	*B. subtilis*	JH642/pAP1	This study	NA
DPH177	*B. subtilis*	DPH105 *amyE*::P_{xyl}-*gfp-orf56 cat*::*spc*	This study	NA
DPH2	*B. subtilis*	JH642/pPW19	This study	NA
DPH3	*B. subtilis*	JH642/pAP6	This study	NA
DPH302	*B. subtilis*	PL1237 *amyE*::P_{xyl}-*gfp-orf56 cat*	This study	NA
DPH324	*B. subtilis*	JH642 *amyE*::P_{spac}-*gfp-orf56 cat*	This study	pDH112
DPH340	*B. subtilis*	JH642 *amyE*::P_{xyl}-*gfp-pbpB cat*	This study	pDH120
DPH371	*B. subtilis*	PL1201 *amyE*::P_{spac}-*orf56 cat*	This study	NA
DPH380	*B. subtilis*	JH642 *amyE*::P_{xyl}-*gfp-ftsW cat*	This study	pDH116
DPH387	*B. subtilis*	DPH380 *cat*::*spc*	This study	NA
DPH400	*B. subtilis*	DPH340 *cat*::*spc*	This study	NA
DPH408	*B. subtilis*	DPH387/pPW19	This study	NA
DPH409	*B. subtilis*	DPH387/pAP6	This study	NA
DPH414	*B. subtilis*	DPH400/pPW19	This study	NA
DPH415	*B. subtilis*	DPH400/pAP6	This study	NA
DPH462	*B. subtilis*	JH642 *thrC*::P_{xyl}-*orf56 erm*	This study	pDH80
DPH50	*B. subtilis*	JH642 *amyE*::P_{xyl}-*gfp-orf56 cat*	This study	pDH81
DPH503	*B. subtilis*	PL1269 *amyE*::P_{xyl}-*gfp-orf56 cat*::*spc*	This study	NA
DPH504	*B. subtilis*	BW121 *amyE*::P_{spac}-*gfp-orf56 cat*	This study	NA
DPH55	*B. subtilis*	PL867 *amyE*::P_{xyl}-*gfp-orf56 cat*	This study	NA
DPH576	*B. subtilis*	JH642 *amyE*::P_{xyl}-*gfp-ftsL cat*	This study	pDH138
DPH579	*B. subtilis*	DPH576 *cat*::*spc*	This study	NA
DPH584	*B. subtilis*	DPH579/pAP6	This study	NA
DPH602	*B. subtilis*	JH642 *amyE*::P_{xyl}-*gfp-divIC cat*	This study	pDH142
DPH614	*B. subtilis*	DPH602 *cat*::*spc*	This study	NA
DPH617	*B. subtilis*	DPH614/pPW19	This study	NA
DPH618	*B. subtilis*	DPH614/pAP6	This study	NA
DPH632	*B. subtilis*	JH642 *amyE*::*divIC cat*	This study	NA
DPH648	*B. subtilis*	DPH632 *cat*::*spc*	This study	NA
DPH660	*B. subtilis*	DPH648/pPW19	This study	NA
DPH661	*B. subtilis*	DPH648/pAP6	This study	NA
DPH79	*B. subtilis*	JH642 *thrC*::P_{spac}-*gfp-divIB erm*	This study	NA
DPH97	*B. subtilis*	DPH79 *amyE*::P_{spac}-*orf56 cat*	This study	NA
JH642	*B. subtilis*	*trpC2 pheA1*	45	NA
KU608	*B. subtilis*	168 *trpC2 metC85*::Tn*917 divIB*::*cat*	54	NA
PL1074	*B. subtilis*	JH642 *ftsAZ*::P_{spac}-*ftsAZ cat*	This study	pPL101
PL108	*B. subtilis*	PY79 *amyE*::*divIC cat*	55	NA
PL1119	*B. subtilis*	JH642 *thrC*::P_{xyl}-*ftsZ erm*	This study	pPL104/pPL106
PL1237	*B. subtilis*	JH642 *divIC*::P_{spac}-*divIC erm*	This study	pDUG1
PL1269	*B. subtilis*	PL1074 *thrC*::P_{xyl}-*ftsZ erm*	This study	NA
PL847	*B. subtilis*	JH642 *ezrA*::*ezrA-gfp spc*	56	NA
PL867	*B. subtilis*	JH642 *ezrA*::*spc*	56	NA
SU633	*B. subtilis*	168 *trpC2 thrC*::P_{spac}-*gfp-divIB erm*	E. Harry	NA
AG1111	*E. coli*	MC1061 F′ $lacI^q$ *lacZ*M15 Tn*10*	46	NA
DHM1	*E. coli*	F^- *cya-854 recA1 endA1 gyrA96 thi1 hsdR17 spoT1 rfbD1 glnV44(AS)*	34	NA
DPH1183	*E. coli*	DHM1/pDH183/pKT25	This study	NA
DPH1164	*E. coli*	DHM1/pDH183/pDH186	This study	NA
DPH1165	*E. coli*	DHM1/pDH183/pDH187	This study	NA
DPH1166	*E. coli*	DHM1/pDH183/pDH188	This study	NA
DPH1167	*E. coli*	DHM1/pDH183/pDH189	This study	NA
DPH1193	*E. coli*	DHM1/pDH183/pDH194	This study	NA
DPH1206	*E. coli*	DHM1/pDH183/pDH195	This study	NA
DPH1185	*E. coli*	DHM1/pDH192/pKT25	This study	NA

(Continued on next page)

TABLE 1 (Continued)

Strain name	Species	Genotype	Source or reference	Plasmid intermediate[a]
DPH1186	*E. coli*	DHM1/pDH192/pDH186	This study	NA
DPH1187	*E. coli*	DHM1/pDH192/pDH187	This study	NA
DPH1197	*E. coli*	DHM1/pDH192/pDH188	This study	NA
DPH1198	*E. coli*	DHM1/pDH192/pDH189	This study	NA
DPH1199	*E. coli*	DHM1/pDH192/pDH194	This study	NA
DPH1209	*E. coli*	DHM1/pDH192/pDH195	This study	NA
DPH1172	*E. coli*	DHM1/pDH190/pKT25	This study	NA
DPH1173	*E. coli*	DHM1/pDH190/pDH186	This study	NA
DPH1174	*E. coli*	DHM1/pDH190/pDH187	This study	NA
DPH1175	*E. coli*	DHM1/pDH190/pDH188	This study	NA
DPH1176	*E. coli*	DHM1/pDH190/pDH189	This study	NA
DPH1177	*E. coli*	DHM1/pDH190/pDH194	This study	NA
DPH1207	*E. coli*	DHM1/pDH190/pDH195	This study	NA

[a]NA, not applicable.

For all experiments, overnight cultures of strains were diluted into fresh LB medium and cultured to mid-exponential growth, monitored as the optical density at 600 nm (OD_{600}) with a Hitachi U-1800 spectrophotometer. Cultures were then diluted a second time to an OD_{600} of 0.025 to 0.05 under appropriate experimental conditions. These cultures were then grown to an OD_{600} between 0.4 and 0.6 and harvested for analysis by microscopy, fixation, or plating as described below.

TABLE 2 Plasmids used in this study

Plasmid name	Description	Oligonucleotides used (forward/reverse)[a]	Source or reference
pAG58	pSI-1/pJH101 derivative with IPTG-inducible P_{spac} for targeted integration of choice	NA	57
pAP1	pPW19-*orf58-orf57-orf56*	NA	18
pAP6	pPW19-*orf56*	NA	18
pDH112	pDR67-*gfp-orf56*	oDH306/oDH148	This study
pDH116	pEA18-*ftsW*	oDH252/oDH253	This study
pDH120	pEA18-*pbpB*	oDH262/oDH263	This study
pDH138	pEA18-*ftsL*	oDH292/oDH293	This study
pDH142	pEA18-*divIC*	oDH294/oDH295	This study
pDH183	pUT18C-*orf56*	oDH439/oDH440	This study
pDH192	pUT18C-*orf56Δ65*	oDH439/oDH440	This study
pDH190	pUT18C-*ftsL*	oDH433/oDH434	This study
pDH186	pKT25-*ftsL*	oDH432/oDH434	This study
pDH187	pKT25-*divIC*	oDH435/oDH437	This study
pDH188	pKT25-*orf56*	oDH438/oDH440	This study
pDH189	pKT25-*orf56Δ65*	oDH438/oDH440	This study
pDH194	pKT25-*divIB*	oDH472/oDH474	This study
pDH195	pKT25-*ftsW*	oDH475/oDH477	This study
pDH80	pRDC19-*orf56*	oDH149/oDH148	This study
pDH81	pEA18-*orf56*	oDH147/oDH148	This study
pDH83	pDR67-*orf56*	oDH149/oDH148	This study
pDH89	pPW19-*orf56Δ65*	NA	This study
pDH91	pEA18-*orf56Δ65*	oDH147/oDH148	This study
pDH92	pDR67-*orf56Δ65*	oDH149/oDH157	This study
pDR67	pAG58 derivative integrative to *amyE* locus with IPTG-inducible P_{spac}	NA	46
pDUG1	pRS14-$divIC_{5'\text{-}3'}$	*divIC*-5′/*divIC*-3′	This study
pEA18	pRDC18 derivative with *spoVG* ribosome binding site followed by *gfp* and in-frame NotI site	NA	58
pJL62	pJH101 derivative for conversion of chloramphenicol-resistant spectinomycin-sensitive strains to chloramphenicol-sensitive spectinomycin-resistant strains	NA	50
pKT25	pSU40 derivative for in-frame 3′-end fusions to *cyaA* for BACTH analysis	NA	34
pPL101	pAG58-$ftsA_{5'\text{-}3'}$	*ftsA*-5′/*ftsA*-3′	This study
pPL104	pUC19-*ftsZ*	*ftsZ*-F4/*ftsZ*-R1	This study
pPL106	pRDC19-*ftsZ*	NA	This study
pPW19	pSI-1 derivative with pUB110 origin with IPTG-inducible P_{spac}	NA	59
pRDC18	pRDC9/pDG1662 derivative integrative to *amyE* locus with xylose-inducible P_{xyl}	NA	F. Arigoni
pRDC19	pRDC9/pDG1664 derivative integrative to *thrC* locus with xylose-inducible P_{xyl}	NA	F. Arigoni
pRS14	pAG58 derivative with *erm* cassette in place of original *cat* cassette	NA	A. Grossman
pUC19	Standard cloning vector	NA	60
pUT18C	pUC19 derivative for in-frame 3′-end fusions to *cyaA* for BACTH analysis	NA	34

[a]NA, not applicable.

TABLE 3 Oligonucleotides used in this study

Oligonucleotide name	Sequence	Target	Restriction site
divIC-3′	GATCGCATGCTGCACTAAGGGAAGATGTTTGG	*divIC*	SphI
divIC-5′	GATCAAGCTTCATAAGAACGACCATCACACGG	*divIC*	HindIII
ftsA-3′	GATCGCATGCGAATTTCTTTATTTTCACTGG	*ftsA*	SphI
ftsA-5′	GATCAAGCTTGTTCCGCAAATAATAGAATAG	*ftsA*	HindIII
ftsZ-F4	GATCGCTAGCCTATTAAGCATGTTTTGGGAATAG	*ftsZ*	HindIII (blunt)
ftsZ-R1	GATCGGATCCCGATTTTGTCCTTTACATTAGC	*ftsZ*	BamHI
oDH147	GATCGCGGCCGCTTTAAATATACAGATCGTTCAGTACGTCAATACATTG	*orf56*	NotI
oDH148	GATCGGATCCTCAGTTACGAGCGGCTTCCTG	*orf56*	BamHI
oDH149	GATCAAGCTTACAGGGGGAATATACATATGTTTAAATATACAGATCGTTCAGTACGTCAATAC	*orf56*	HindIII
oDH157	GATCGCATGCTCAGTTACGAGCGGCTTC	*orf56*	SphI
oDH252	GATCGCGGCCGCTTAAAAAAAATGCTAAAATCTTATGATTACTCACTGATATTCG	*ftsW*	NotI
oDH253	GATCGGATCCCCCTGTACACACTTGTTTTTTACAGATAAACAG	*ftsW*	BamHI
oDH262	GATAGCGGCCGCATTCAAATGCCAAAAAAGAATAAATTTATGAATAGAG	*pbpB*	NotI
oDH263	GATAGGATCCCATAACGACGGCTTTCTTTTTAATCAGG	*pbpB*	BamHI
oDH292	CTAAGCGGCCGCAGCAATTTAGCTTACCAACC	*ftsL*	NotI
oDH293	GATTGGATCCGGCATTTGAATCATTCCTGTATG	*ftsL*	BamHI
oDH294	CTAAGCGGCCGCAATTTTTCCAGGGAACGAAC	*divIC*	NotI
oDH295	GATTGGATCCGTGTCAACAAGGCTACTTG	*divIC*	BamHI
oDH306	GATTAAGCTTGGGAAAAGGTGGTGAACTACTATG	RBS_{spoVG}-*gfp*	HindIII
oDH432	TGTACTGCAGGGAGCAATTTAGCTTACCAACCAGAGAAACAG	*ftsL*	PstI
oDH433	TACACTGCAGGAGCAATTTAGCTTACCAACCCAGAGAAACAG	*ftsL*	PstI
oDH434	TAACCCCGGGTCATTCCTGTATGTTTTTCACTTTTTTATCTTTAAATTCAAG	*ftsL*	BamHI
oDH435	CGTACTGCAGGGAATTTTTCCAGGGAACGAACGATAACTG	*divIC*	PstI
oDH437	CCTCCCCGGGCTACTTGCTCTTCTTCTCCACATTGAAGATAACTTCTC	*divIC*	BamHI
oDH438	TCTGCTGCAGGGTTTAAATATACAGATCGTTCAGTACGTCAATACATTGAAAGA	*orf56*	PstI
oDH439	GCCACTGCAGGTTTAAATATACAGATCGTTCAGTACGTCAATACATTGAAAGA	*orf56*	PstI
oDH440	ATCGCCCGGGTCAGTTACGAGCGGCTTCCTGA	*orf56*	BamHI
oDH472	GATTCTGCAGGGATGAACCCGGGTCAAGACC	*divIB*	PstI
oDH474	GATTCCCGGTCAATTTTCATCCTTCCTTTTTAGCAG	*divIB*	BamHI
oDH475	GATTCTGCAGGGATGTTAAAAAAAATGCTAAAATCTTATGATTACTG	*ftsW*	PstI
oDH477	GATTCCCGGTTACAGATAAACAGTTTTTTTGAGCTGTTTC	*ftsW*	BamHI

Plasmid and strain construction. Cloning and genetic manipulation were performed using standard techniques (48, 49) using naturally competent *B. subtilis* cells or chemically competent *E. coli* cells. *Pyrococcus furiosus* DNA polymerase (G-Biosciences) was used for PCRs in an Eppendorf Mastercycler; standard restriction enzymes and T4 DNA polymerase (New England Biolabs) were used for cloning. Plasmid DNA was prepared using the Wizard Plus SV Minipreps DNA purification kit, PCR and digestion reaction mixtures were cleaned up using the Wizard SV gel and PCR cleanup system, and chromosomal DNA was prepared using the Wizard genomic DNA purification kit (Promega).

The final versions of all cloning products were sequenced to verify their construction. DNA sequencing was performed by GENEWIZ (South Plainfield, NJ), SeqWright (Houston, TX), or Psomagen, Inc. (Rockville, MD). DNA bands were visualized using a Gel Doc XR imager (Bio-Rad), and DNA concentrations were estimated with a NanoDrop ND-1000 spectrophotometer (Thermo Fisher Scientific).

All plasmids are listed in Table 2, and oligonucleotides purchased from IDT DNA or Thermo Fisher Scientific and used for their construction are listed in Table 3. Table 2 includes details on which oligonucleotides were used for the cloning of each plasmid new to this study. Table 3 includes details on oligonucleotide sequences, genes targeted for amplification, and restriction sites used in the plasmid construction where appropriate. All *E. coli* strains new to this study, as well as *B. subtilis* strains DPH2, DPH3, and DPH176, were cloned by transformation with plasmids as indicated in Tables 1 and 2. All of the remaining *B. subtilis* strains new to this study were cloned by transformation with plasmids as indicated in Tables 1 and 2, followed by screening for single or double crossover into the *B. subtilis* chromosome. Where appropriate, loss of a plasmid backbone following double crossover was verified by antibiotic counterselection. Successful integrations at *amyE* were verified by iodine staining on starch plates, and testing for threonine auxotrophy was used to verify successful integration at *thrC*. pJL62 (50) was used for conversion of chloramphenicol-resistant spectinomycin-sensitive strains to chloramphenicol-sensitive spectinomycin-resistant ones. Strain PL1119 was created by first cloning *ftsZ* into pUC19 as indicated in Table 2 to create pPL104, followed by subcloning into pRDC19 to create pPL106 for transfer into the *B. subtilis* chromosome. pKT25 and pUT18C (34) were used for BACTH experiments (see below).

Plating efficiency assays. Cells used for dilutions and subsequent CFU counting were taken from fresh cultures grown to an OD_{600} between 0.4 and 0.6 under experimental conditions. Tenfold serial dilutions of these cultures were prepared in 200 μl of fresh LB medium (with or without IPTG as appropriate) in a 96-well plate using a multichannel pipette; 75 μl of these dilutions was then spread-plated on LB medium, with or without IPTG or chloramphenicol, as appropriate. Plates with dilutions that gave rise to well-separated colonies were used for counts, and total CFU were calculated.

Cell fixation, microscopy, and analysis. Cells used for microscopy were taken from fresh cultures grown to an OD_{600} between 0.4 and 0.6 under experimental conditions and then harvested for fixation

or immediate live visualization with differential interference contrast (DIC) microscopy. Prior to microscopy, live cell samples were stained with the vital membrane stain FM4-64 (Molecular Probes). Cell fixation and preparation for IFM, including the antibodies employed, were performed as described previously (22, 23). Images were processed and analyzed for ring frequency and cell width or length (interseptal distance for chains of *B. subtilis* cells) measurements using the ObjectJ extension (51) of ImageJ (52).

Microscopy was performed using a 100× DIC objective on an Olympus BX60 microscope with a Hamamatsu C8484 camera using HC Image software (Hamamatsu), an Olympus BX51 microscope with an OrcaERG camera (Hamamatsu) using Nikon Elements Advanced Research software, or a Nikon Eclipse TE2000-E microscope using MetaVue v7.8 software (Molecular Devices). Images were processed for brightness/contrast and colorization using Adobe Photoshop.

BACTH assays. For BACTH experiments (34), DivIC, FtsL, gp56, gp56Δ65, DivIB, and FtsW were each fused to the carboxyl terminus of T25 from *Bordetella pertussis* in pKT25. Additionally, gp56, gp56Δ65, and FtsL were fused to the carboxyl terminus of T18 from *Bordetella pertussis* in pUT18C. Plasmids were heat shock transformed sequentially into competent DHM1 cells and grown at 30°C. Strains were patched onto medium containing 50 g/ml X-Gal (Gold Biotechnology), 1 mM IPTG, and antibiotics. Patches were screened for a color change following 1.5 days of incubation at 30°C. The liquid-based assay to quantify β-galactosidase activities was performed using 0.4% ONPG exactly according to the protocol published previously (35).

SUPPLEMENTAL MATERIAL

Supplemental material is available online only.

SUPPLEMENTAL FILE 1, PDF file, 0.9 MB.

ACKNOWLEDGMENTS

We thank Fabrizio Arigoni, Alan Grossman, Frederico Gueiros-Filho, Liz Harry, and Joe Lutkenhaus for the kind gift of strains and plasmids. We thank members of the Department of Microbiology and Molecular Genetics at the University of Texas Houston and the members of the Department of Biology at Canisius College for helpful discussions.

This research was made possible through NIH funding to W.M. (grant GM61074) and P.A.L. (grant GM127331), Frieberg Visiting Professor of Biology research funding from the Department of Biology, Washington University in St. Louis, to D.P.H., start-up and departmental research funds from Canisius College to D.P.H., and Canisius Earned Excellence Program (CEEP) undergraduate student research funding to A.B., J.L., S.A., and A.M. I.I. received partial support from the Canisius Science Scholars Program, under an NSF S-STEM award (grant 1643649). Publication costs after acceptance were supported through an Innovation Fund from the National Endowment for the Humanities and the College of Arts & Sciences at Canisius College.

Author contributions were as follows: experiments, A.B., I.I., J.L., and D.P.H.; supporting experiments, S.A., M.B., D.H., A.M., and A.P.; design, funding, and resources, C.R.S., W.M., P.A.L., and D.P.H.; writing, D.P.H.

REFERENCES

1. Haeusser DP, Margolin W. 2016. Splitsville: structural and functional insights into the dynamic bacterial Z ring. Nat Rev Microbiol 14:305–319. https://doi.org/10.1038/nrmicro.2016.26.
2. Trueba FJ. 1982. On the precision and accuracy achieved by *Escherichia coli* cells at fission about their middle. Arch Microbiol 131:55–59. https://doi.org/10.1007/BF00451499.
3. Yu X-C, Margolin W. 1999. FtsZ ring clusters in *min* and partition mutants: role of both the Min system and the nucleoid in regulating FtsZ ring localization. Mol Microbiol 32:315–326. https://doi.org/10.1046/j.1365-2958.1999.01351.x.
4. Du S, Lutkenhaus J. 2019. At the heart of bacterial cytokinesis: the Z ring. Trends Microbiol 27:781–791. https://doi.org/10.1016/j.tim.2019.04.011.
5. Tripathy S, Sahu SK. 2019. FtsZ inhibitors as a new genera of antibacterial agents. Bioorg Chem 91:103169. https://doi.org/10.1016/j.bioorg.2019.103169.
6. Hurley KA, Santos TMA, Nepomuceno GM, Huynh V, Shaw JT, Weibel DB. 2016. Targeting the bacterial division protein FtsZ. J Med Chem 59:6975–6998. https://doi.org/10.1021/acs.jmedchem.5b01098.
7. Wang M, Fang C, Ma B, Luo X, Hou Z. 2020. Regulation of cytokinesis: FtsZ and its accessory proteins. Curr Genet 66:43–49. https://doi.org/10.1007/s00294-019-01005-6.
8. Wang X, Kim Y, Ma Q, Hong SH, Pokusaeva K, Sturino JM, Wood TK. 2010. Cryptic prophages help bacteria cope with adverse environments. Nat Commun 1:147. https://doi.org/10.1038/ncomms1146.
9. Balasubramanian D, Ragunathan PT, Fei J, Vanderpool CK. 2016. A prophage-encoded small RNA controls metabolism and cell division in *Escherichia coli*. mSystems 1:e00021-15. https://doi.org/10.1128/mSystems.00021-15.
10. Rowlett VW, Margolin W. 2015. The Min system and other nucleoid-independent regulators of Z ring positioning. Front Microbiol 6:478. https://doi.org/10.3389/fmicb.2015.00478.
11. Johnson JE, Lackner LL, Hale CA, de Boer PAJ. 2004. ZipA is required for targeting of DMinC/DicB, but not DMinC/MinD, complexes to septal ring assemblies in *Escherichia coli*. J Bacteriol 186:2418–2429. https://doi.org/10.1128/jb.186.8.2418-2429.2004.
12. Ragunathan PT, Vanderpool CK. 2019. Cryptic-prophage-encoded small protein DicB protects *Escherichia coli* from phage infection by inhibiting inner membrane receptor proteins. J Bacteriol 201:e00475-19. https://doi.org/10.1128/JB.00475-19.
13. Conter A, Bouché JP, Dassain M. 1996. Identification of a new inhibitor of essential division gene *ftsZ* as the *kil* gene of defective prophage Rac.

J Bacteriol 178:5100–5104. https://doi.org/10.1128/jb.178.17.5100-5104.1996.
14. Kiro R, Molshanski-Mor S, Yosef I, Milam SL, Erickson HP, Qimron U. 2013. Gene product 0.4 increases bacteriophage T7 competitiveness by inhibiting host cell division. Proc Natl Acad Sci U S A 110:19549–19554. https://doi.org/10.1073/pnas.1314096110.
15. Haeusser DP, Hoashi M, Weaver A, Brown N, Pan J, Sawitzke JA, Thomason LC, Court DL, Margolin W. 2014. The Kil peptide of bacteriophage lambda blocks *Escherichia coli* cytokinesis via ZipA-dependent inhibition of FtsZ assembly. PLoS Genet 10:e1004217. https://doi.org/10.1371/journal.pgen.1004217.
16. Hernández-Rocamora VM, Alfonso C, Margolin W, Zorrilla S, Rivas G. 2015. Evidence that bacteriophage λ Kil peptide inhibits bacterial cell division by disrupting FtsZ protofilaments and sequestering protein subunits. J Biol Chem 290:20325–20335. https://doi.org/10.1074/jbc.M115.653329.
17. Stewart CR, Casjens SR, Cresawn SG, Houtz JM, Smith AL, Ford ME, Peebles CL, Hatfull GF, Hendrix RW, Huang WM, Pedulla ML. 2009. The genome of *Bacillus subtilis* bacteriophage SPO1. J Mol Biol 388:48–70. https://doi.org/10.1016/j.jmb.2009.03.009.
18. Stewart CR, Deery WJ, Egan ESK, Myles B, Petti AA. 2013. The product of SPO1 gene 56 inhibits host cell division during infection of *Bacillus subtilis* by bacteriophage SPO1. Virology 447:249–253. https://doi.org/10.1016/j.virol.2013.09.005.
19. Rowlett VW, Margolin W. 2015. The bacterial divisome: ready for its close-up. Philos Trans R Soc B 370:20150028. https://doi.org/10.1098/rstb.2015.0028.
20. Errington J, Wu LJ. 2017. Cell cycle machinery in *Bacillus subtilis*, p 67–101. *In* Löwe J, Amos LA (ed), Prokaryotic cytoskeletons: filamentous protein polymers active in the cytoplasm of bacterial and archaeal cells. Springer International Publishing, Cham, Switzerland.
21. Duman R, Ishikawa S, Celik I, Strahl H, Ogasawara N, Troc P, Löwe J, Hamoen LW. 2013. Structural and genetic analyses reveal the protein SepF as a new membrane anchor for the Z ring. Proc Natl Acad Sci U S A 110:E4601–E4610. https://doi.org/10.1073/pnas.1313978110.
22. Haeusser DP, Schwartz RL, Smith AM, Oates ME, Levin PA. 2004. EzrA prevents aberrant cell division by modulating assembly of the cytoskeletal protein FtsZ. Mol Microbiol 52:801–814. https://doi.org/10.1111/j.1365-2958.2004.04016.x.
23. Haeusser DP, Garza AC, Buscher AZ, Levin PA. 2007. The division inhibitor EzrA contains a seven-residue patch required for maintaining the dynamic nature of the medial FtsZ ring. J Bacteriol 189:9001–9010. https://doi.org/10.1128/JB.01172-07.
24. Wadsworth KD, Rowland SL, Harry EJ, King GF. 2008. The divisomal protein DivIB contains multiple epitopes that mediate its recruitment to incipient division sites. Mol Microbiol 67:1143–1155. https://doi.org/10.1111/j.1365-2958.2008.06114.x.
25. Daniel RA, Harry EJ, Katis VL, Wake RG, Errington J. 1998. Characterization of the essential cell division gene *ftsL* (*yllD*) of *Bacillus subtilis* and its role in the assembly of the division apparatus. Mol Microbiol 29:593–604. https://doi.org/10.1046/j.1365-2958.1998.00954.x.
26. Katis VL, Harry EJ, Wake RG. 1997. The *Bacillus subtilis* division protein DivIC is a highly abundant membrane-bound protein that localizes to the division site. Mol Microbiol 26:1047–1055. https://doi.org/10.1046/j.1365-2958.1997.6422012.x.
27. Daniel RA, Errington J. 2000. Intrinsic instability of the essential cell division protein FtsL of *Bacillus subtilis* and a role for DivIB protein in FtsL turnover. Mol Microbiol 36:278–289. https://doi.org/10.1046/j.1365-2958.2000.01857.x.
28. Daniel RA, Noirot-Gros M-F, Noirot P, Errington J. 2006. Multiple interactions between the transmembrane division proteins of *Bacillus subtilis* and the role of FtsL instability in divisome assembly. J Bacteriol 188:7396–7404. https://doi.org/10.1128/JB.01031-06.
29. Gamba P, Hamoen LW, Daniel RA. 2016. Cooperative recruitment of FtsW to the division site of *Bacillus subtilis*. Front Microbiol 7:1808. https://doi.org/10.3389/fmicb.2016.01808.
30. Arjes HA, Kriel A, Sorto NA, Shaw JT, Wang JD, Levin PA. 2014. Failsafe mechanisms couple division and DNA replication in bacteria. Curr Biol 24:2149–2155. https://doi.org/10.1016/j.cub.2014.07.055.
31. Letunic I, Bork P. 2018. 20 years of the SMART protein domain annotation resource. Nucleic Acids Res 46:D493–D496. https://doi.org/10.1093/nar/gkx922.
32. Ikeda M, Arai M, Okuno T, Shimizu T. 2003. TMPDB: a database of experimentally-characterized transmembrane topologies. Nucleic Acids Res 31:406–409. https://doi.org/10.1093/nar/gkg020.
33. Levin PA. 2002. Light microscopy techniques for bacterial cell biology. Methods Microbiol 31:115–132. https://doi.org/10.1016/S0580-9517(02)31007-9.
34. Karimova G, Pidoux J, Ullmann A, Ladant D. 1998. A bacterial two-hybrid system based on a reconstituted signal transduction pathway. Proc Natl Acad Sci U S A 95:5752–5756. https://doi.org/10.1073/pnas.95.10.5752.
35. Karimova G, Dautin N, Ladant D. 2005. Interaction network among *Escherichia coli* membrane proteins involved in cell division as revealed by bacterial two-hybrid analysis. J Bacteriol 187:2233–2243. https://doi.org/10.1128/JB.187.7.2233-2243.2005.
36. Simpkin AJ, Rigden DJ. 2016. GP0.4 from bacteriophage T7: in silico characterisation of its structure and interaction with *E. coli* FtsZ. BMC Res Notes 9:343. https://doi.org/10.1186/s13104-016-2149-5.
37. Kawai Y, Moriya S, Ogasawara N. 2003. Identification of a protein, YneA, responsible for cell division suppression during the SOS response in *Bacillus subtilis*. Mol Microbiol 47:1113–1122. https://doi.org/10.1046/j.1365-2958.2003.03360.x.
38. Ballesteros-Plaza D, Holguera I, Scheffers D-J, Salas M, Muñoz-Espín D. 2013. Phage ϕ29 protein p1 promotes replication by associating with the FtsZ ring of the divisome in *Bacillus subtilis*. Proc Natl Acad Sci U S A 110:12313–12318. https://doi.org/10.1073/pnas.1311524110.
39. Wagner-Herman JK, Bernard R, Dunne R, Bisson-Filho AW, Kumar K, Nguyen T, Mulcahy L, Koullias J, Gueiros-Filho FJ, Rudner DZ. 2012. RefZ facilitates the switch from medial to polar division during spore formation in *Bacillus subtilis*. J Bacteriol 194:4608–4618. https://doi.org/10.1128/JB.00378-12.
40. Brown EE, Miller AK, Krieger IV, Otto RM, Sacchettini JC, Herman JK. 2019. A DNA-binding protein tunes septum placement during *Bacillus subtilis* sporulation. J Bacteriol 201:e00287-19. https://doi.org/10.1128/JB.00287-19.
41. Tsang M-J, Bernhardt TG. 2015. A role for the FtsQLB complex in cytokinetic ring activation revealed by an *ftsL* allele that accelerates division. Mol Microbiol 95:925–944. https://doi.org/10.1111/mmi.12905.
42. den Blaauwen T, Luirink J. 2019. Checks and balances in bacterial cell division. mBio 10:e00149-19. https://doi.org/10.1128/mBio.00149-19.
43. Pichoff S, Du S, Lutkenhaus J. 2018. Disruption of divisome assembly rescued by FtsN-FtsA interaction in *Escherichia coli*. Proc Natl Acad Sci U S A 115:E6855–E6862. https://doi.org/10.1073/pnas.1806450115.
44. Busiek KK, Eraso JM, Wang Y, Margolin W. 2012. The early divisome protein FtsA interacts directly through its 1c subdomain with the cytoplasmic domain of the late divisome protein FtsN. J Bacteriol 194:1989–2000. https://doi.org/10.1128/JB.06683-11.
45. Perego M, Spiegelman GB, Hoch JA. 1988. Structure of the gene for the transition state regulator, *abrB*: regulator synthesis is controlled by the *spo0A* sporulation gene in *Bacillus subtilis*. Mol Microbiol 2:689–699. https://doi.org/10.1111/j.1365-2958.1988.tb00079.x.
46. Ireton K, Rudner DZ, Siranosian KJ, Grossman AD. 1993. Integration of multiple developmental signals in *Bacillus subtilis* through the Spo0A transcription factor. Genes Dev 7:283–294. https://doi.org/10.1101/gad.7.2.283.
47. Haeusser DP, Rowlett VW, Margolin W. 2015. A mutation in *Escherichia coli ftsZ* bypasses the requirement for the essential division gene *zipA* and confers resistance to FtsZ assembly inhibitors by stabilizing protofilament bundling. Mol Microbiol 97:988–1005. https://doi.org/10.1111/mmi.13081.
48. Harwood CR, Cutting SM (ed). 1990. Molecular biological methods for Bacillus. Wiley, Chichester; England.
49. Sambrook J, Russell DW. 2001. Molecular cloning: a laboratory manual. Cold Spring Harbor Laboratory Press, Cold Spring Harbor, NY.
50. LeDeaux JR, Grossman AD. 1995. Isolation and characterization of *kinC*, a gene that encodes a sensor kinase homologous to the sporulation sensor kinases KinA and KinB in *Bacillus subtilis*. J Bacteriol 177:166–175. https://doi.org/10.1128/jb.177.1.166-175.1995.
51. van der Ploeg R, Verheul J, Vischer NOE, Alexeeva S, Hoogendoorn E, Postma M, Banzhaf M, Vollmer W, den Blaauwen T. 2013. Colocalization and interaction between elongasome and divisome during a preparative cell division phase in *Escherichia coli*. Mol Microbiol 87:1074–1087. https://doi.org/10.1111/mmi.12150.
52. Schneider CA, Rasband WS, Eliceiri KW. 2012. NIH Image to ImageJ: 25 years of image analysis. Nat Methods 9:671–675. https://doi.org/10.1038/nmeth.2089.
53. Weart RB, Levin PA. 2003. Growth rate-dependent regulation of

medial FtsZ ring formation. J Bacteriol 185:2826–2834. https://doi.org/10.1128/JB.185.9.2826-2834.2003.
54. Beall B, Lutkenhaus J. 1989. Nucleotide sequence and insertional inactivation of a *Bacillus subtilis* gene that affects cell division, sporulation, and temperature sensitivity. J Bacteriol 171:6821–6834. https://doi.org/10.1128/jb.171.12.6821-6834.1989.
55. Levin PA, Losick R. 1994. Characterization of a cell division gene from *Bacillus subtilis* that is required for vegetative and sporulation septum formation. J Bacteriol 176:1451–1459. https://doi.org/10.1128/jb.176.5.1451-1459.1994.
56. Levin PA, Kurtser IG, Grossman AD. 1999. Identification and characterization of a negative regulator of FtsZ ring formation in *Bacillus subtilis*. Proc Natl Acad Sci U S A 96:9642–9647. https://doi.org/10.1073/pnas.96.17.9642.
57. Jaacks KJ, Healy J, Losick R, Grossman AD. 1989. Identification and characterization of genes controlled by the sporulation-regulatory gene spo0H in *Bacillus subtilis*. J Bacteriol 171:4121–4129. https://doi.org/10.1128/jb.171.8.4121-4129.1989.
58. Fujita M, Losick R. 2002. An investigation into the compartmentalization of the sporulation transcription factor σE in *Bacillus subtilis*. Mol Microbiol 43:27–38. https://doi.org/10.1046/j.1365-2958.2002.02732.x.
59. Wei P, Stewart CR. 1993. A cytotoxic early gene of *Bacillus subtilis* bacteriophage SPO1. J Bacteriol 175:7887–7900. https://doi.org/10.1128/jb.175.24.7887-7900.1993.
60. Norrander J, Kempe T, Messing J. 1983. Construction of improved M13 vectors using oligodeoxynucleotide-directed mutagenesis. Gene 26:101–106. https://doi.org/10.1016/0378-1119(83)90040-9.